RESEARCH ARTICLE | MAY 22 2023

Supercurrent diode effect in thin film Nb tracks

N Satchell ; PM Shepley ; MC Rosamond; G Burnell

Journal of Applied Physics 133, 203901 (2023)
https://doi.org/10.1063/5.0141576

Journal of Applied Physics ARTICLE scitation.org/journal/jap

Supercurrent diode effect in thin film Nb tracks

Cite as: J. Appl. Phys. **133**, 203901 (2023); doi: 10.1063/5.0141576
Submitted: 15 February 2023 · Accepted: 5 May 2023 ·
Published Online: 22 May 2023

N Satchell,[1,a)] PM Shepley,[1] MC Rosamond,[2] and G Burnell[1,b)]

AFFILIATIONS

[1]School of Physics and Astronomy, University of Leeds, Leeds LS2 9JT, United Kingdom
[2]School of Electronic and Electrical Engineering, University of Leeds, Leeds LS2 9JT, United Kingdom

[a)]**Author to whom correspondence should be addressed:** N.D.Satchell@leeds.ac.uk
[b)]**Electronic mail:** g.burnell@leeds.ac.uk

ABSTRACT

We demonstrate nonreciprocal critical current in 65 nm thick polycrystalline and epitaxial Nb thin films patterned into tracks. The nonreciprocal behavior gives a supercurrent diode effect, where the current passed in one direction is a supercurrent and the other direction is a normal state (resistive) current. We attribute fabrication artifacts to creating the supercurrent diode effect in our tracks. We study the variation of the diode effect with temperature and the magnetic field and find a dependence with the width of the Nb tracks from 2 to 10 μm. For both polycrystalline and epitaxial samples, we find that tracks of width 4 μm provide the largest supercurrent diode efficiency of up to $\approx$30%, with the effect reducing or disappearing in the widest tracks of 10 μm. We propose a model based on the limiting contributions to the critical current density to explain the track width dependence of the induced supercurrent diode effect. It is anticipated that the supercurrent diode will become a ubiquitous component of the superconducting computer.

I. INTRODUCTION

The supercurrent diode is an analog to rectification in semiconductor pn junctions, where current is allowed to flow only in one direction. In the supercurrent diode, the critical current of the device (I_c) is nonreciprocal ($I_c^+ \neq I_c^-$), leading to the situation where a dissipationless supercurrent can pass in one direction, but upon reversing the current direction, the device becomes resistive. It has been suggested that a supercurrent diode may become a useful component for digital processing in a superconducting computer.

Nonreciprocal I_c behavior has been predicted and observed prior to the common use of the term supercurrent diode effect. Some notable early experimental works include superconducting foils under external magnetic fields[1] and reports in superconductor–ferromagnet hybrid systems.[2–5]

Theoretically, a nonreciprocal I_c can manifest in Josephson devices with anomalous ϕ_0 phase differences[6,7] or when the barrier materials have symmetry breaking.[8,9] A common requirement of such predictions is that the barriers contain exotic materials such as ferromagnetic multilayers,[10–16] topological insulators,[17–19] Weyl semimetals,[20–23] materials with large spin-orbit coupling,[24–26] or that the electrodes are unconventional superconductors.[27–29] Several recent experiments have reported the Josephson diode effect in devices with exotic barrier materials.[30–35]

In addition to the Josephson diode effect are reports and predictions for an intrinsic supercurrent diode effect. Theoretically, an intrinsic effect can occur in superconducting material systems with symmetry breaking, such as broken inversion symmetry[36–40] or broken time-reversal symmetry.[37,41,42] Therefore, much attention has been paid to observations of the supercurrent diode effect in exotic materials systems such as multilayers with noncentrosymmetric structure[43–46] and systems with time-reversal symmetry breaking.[47] In order to fully understand the interesting and novel new physics of such systems, it is important to be able to distinguish between the supercurrent diode effect, which is intrinsic to the material and which is induced as a result of device fabrication.

An induced supercurrent diode effect can occur in tracks of *s*-wave superconductors without intrinsic inversion or time-reversal symmetry breaking, such as Nb.[48–51] The induced supercurrent diode effect is attributed to non-perfect device fabrication leading to imperfections in the edges of the tracks. Therefore, the edges of the tracks are unlikely to be identical, which can lead to the unequal generation, penetration, and expulsion of vortices on the opposite edges of the tracks, resulting in rectification.[48,52]

The ability to induce a supercurrent diode effect without requirements for exotic materials is useful from a practical point of view since established industrial processes tend to be based on *s*-wave superconductors such as Nb.

In this work, we report measurements on Nb thin films patterned into tracks of varying widths. From our field and temperature dependent measurements of the induced supercurrent diode effect, we report three key experimental observations. First, our Nb tracks are 65 nm thick, refining the thickness in which the supercurrent diode effect manifests. Second, by varying the width of the tracks, we observe a dependence on the diode effect with track width. Third, we establish that single crystal epitaxy is not a condition for the diode effect by measuring both polycrystalline and epitaxial samples. We report our observed diode effect as an efficiency parameter $\eta = \frac{I_c^+ - I_c^-}{I_c^+ + I_c^-}$. Finally, we propose a model to explain our observed track width dependence in terms of the critical current densities in our devices and conclude that the induced supercurrent diode effect is a particularly important consideration in track widths where vortex penetration contributes significantly to the overall critical current density.

II. METHODS

Nb films are deposited by dc magnetron sputtering in the Royce Deposition System.[53] The magnetrons are mounted below, and confocal to, the substrate with source–substrate distances of 134 mm. The base pressure of the vacuum chamber is 3×10^{-9} mBar with the substrate at room temperature and 1×10^{-8} mBar with the substrate at 1000°C. Nb is grown at a rate of 0.06 nm/s at an Ar (6N purity) gas pressure of 3.6×10^{-3} mBar to a nominal thickness of 65 nm. The growth rate and film thicknesses are checked by x-ray reflectivity. The first Nb sample was deposited at room temperature on the Si/SiO_x substrate, and the second Nb sample was deposited at an elevated temperature of 1000°C onto a single crystal *a*-plane Al_2O_3 substrate to promote epitaxial growth.

Samples are fabricated into tracks using a direct laser writer to define resist masks in the S1813 photoresist, and reactive ion etching at 130 W in a 1:2 Ar:SF6 plasma to etch the Nb films. After fabrication, devices are measured in a continuous flow ^{4}He cryostat with 3 T horizontal superconducting Helmholtz coils. Traditional 4-point-probe transport geometry is used to measure the current–voltage characteristic of the tracks with a combined Keithley 6221-2182A current source and nano-voltmeter in pulse mode with 1 ms pulses and a 1% duty cycle to avoid a reduced retracking I_c due to heating. Varying the duty cycle from 1% to 50% resulted in no changes to the reported I_c. The schematic of the fabricated devices and measurement geometry is shown in Fig. 1(a).

The sample grown at room temperature has a superconducting T_c of 8.75 K and a residual-resistivity ratio (*RRR*) of 2.8, giving an estimate for the mean free path (ℓ) of 6 nm—indicating a polycrystalline microsctructure. The second sample has a higher T_c of 9.05 K and a *RRR* of 30, giving an estimate for ℓ of 96 nm, consistent with an epitaxial microstructure. The increased ℓ is expected for the epitaxial Nb due to the decrease in crystallographic defects such as grain boundaries. The properties of our polycrystalline Nb thin films are reported elsewhere.[54]

III. RESULTS

Figure 1 shows the supercurrent diode effect in the polycrystalline sample with 4 μm wide track. Figure 1(b) shows the current–voltage (*I*–*V*) characteristic of our track at applied fields where the diode effect is found to be maximum. I_c^+ and I_c^- are extracted from the *I*–*V* when the voltage reaches a small threshold value. Large nonreciprocal I_c^+ and I_c^- can be seen in the *I*–*V* characteristic. When the field polarity is reversed, the nonreciprocal I_c^+ and I_c^- are also reversed. In the normal state of the device, the *I*–*V* curve shows a slight non-linear dependence, which we attribute to Joule heating as a result of the large current densities. Our measurements at lower current densities (e.g., in wider tracks or at warmer temperatures) show *I*–*V* curves following the expected linear metallic behavior.

Figure 1(c) shows the out-of-plane applied field dependence of I_c^+ and I_c^-. Due to the diode effect, unexpectedly, the maximum values of I_c do not occur at the zero applied field. We attribute this to the vortex penetration field, which is discussed later. The presented field sweep is acquired by sweeping from the negative to the positive field. A similar curve with the same features is obtained by sweeping from the positive to negative field. The sign of the I_c^+/I_c^- maximum with the positive/negative field does not change with temperature or the field sweep direction and appears to favor having the I_c^+ (I_c^-) maximum in the positive (negative) field. Across the 11 samples in our study showing the diode effect, when keeping the device mounting and wiring geometry the same, I_c^+ (I_c^-) maximum appears in the positive (negative) field with a ratio of 8:3. The I_c^+/I_c^- maximum with positive/negative field can be reversed by swapping the current wiring direction [Fig. 1(a)]. Figure 1(d) shows the extracted diode efficiency η, where peak efficiency is achieved around the fields corresponding to I_c^+/I_c^- maximum. The maximum in η corresponding to the maximum in I_c^+ is a common feature of our data, however, we believe that this is a consequence of how η is defined rather than being a fundamental feature of the induced supercurrent diode. We note a sight asymmetry and digitization in the high field η values in this device, Fig. 1(d). The asymmetry in η at high fields is present in some of our devices and may indicate that the diode effect persists to high fields in some devices. The digitization of η at high fields is a result of determining I_c from the finite current step size in the I–V measurements.

Our interpretation of the origin of the supercurrent diode effect relies upon our samples being in the limit where the critical current is determined by the vortices in the system, as opposed to being the depairing current. From the $I_c(B)$ dependence, it is possible to extract the maximum super-heating field of the Meissner state,[48] B_s. The inset to Fig. 1(c) shows the low field I_c with linear fits (dashed lines). B_s corresponds to the interpolated intercept of the fits to the low field data, when the *B* offset is taken into account. From the four linear fits shown in Fig. 1(c) inset, we obtain $B_s = 10 \pm 1$ mT. The expression,[48] $B_s = \phi_0/(\sqrt{3}\pi\xi w)$, provides an order of magnitude estimate for B_s, where ϕ_0 is the flux quantum and ξ is the Ginzburg–Landau coherence length ($\xi = 11.6$ nm for polycrystalline thin film Nb[54]). For $w = 4\,\mu$m, $B_s = 8.2$ mT, in approximate agreement with our experimental findings. This indicates strongly that in the region where the diode effect is observed the critical current is determined by the vorticies.

Figure 2(a) shows a scanning electron microscope image of the epitaxial 65 nm thick Nb sample patterned into 4 μm wide track. To avoid charging during imaging, a thin Au layer is deposited over the whole sample. Imaging of multiple tracks reveals the following: first, some hardened resist residue remains on the devices at the sidewalls. We do not believe that the resist residue contributes to the observed diode effect; second, all our devices have a low line-edge roughness in the range of 10–40 nm with no significant differences between opposite edges. This implies that the fabrication artifacts believed to be responsible for the induced diode effect are subtle.

Figure 2 shows the supercurrent diode effect in the epitaxial 65 nm thick Nb sample patterned into 4 μm wide track at 5 K. From the comparison with the polycrystalline device presented in Fig. 1 of the same track width and measurement temperature, the epitaxial device shares many of the same features with the following differences. From the I-V characteristic, Fig. 2(b), the residual resistance of the epitaxial sample is lower than the polycrystalline sample. This sample also displays slightly non-linear dependence, consistent with Joule heating. The tracks patterned from the epitaxial sample have an I_c about twice that of the polycrystalline track, shown in Figs. 2(b) and 2(c). The increased I_c in the epitaxial sample is most likely due to the combination of increased gap (higher T_c), decreased grain boundaries, and increased mean free path compared to the polycrystalline sample. As shown in Fig. 2(d), the measured maximum η in this condition is smaller than the polycrystalline sample.

We next study the track width dependence of the supercurrent diode effect in the polycrystalline and epitaxial Nb samples. For polycrystalline Nb, the London penetration depth $\lambda_L = 96$ nm,[54] providing an estimate of the Pearl penetration depth $\lambda_P = 2\lambda_L^2/t \approx 300$ nm. For comparable epitaxial Nb, λ_L tends toward bulk[55] providing an estimate $\lambda_P \approx 50$ nm. Other works have considered tracks in the limit $w/\lambda_P = 1/25$[49] and $w/\lambda_P = 2$;[48] however, here we explore a new limit where the width of the tracks is far greater than the Pearl penetration depth, $w \gg \lambda_P$, covering between $10 < w/\lambda_P < 200$. In this new limit, we observe a significant superconducting diode effect and report a width dependence in our samples.

Figure 3 shows the full track width and temperature dependence of the supercurrent diode effect in the epitaxial and

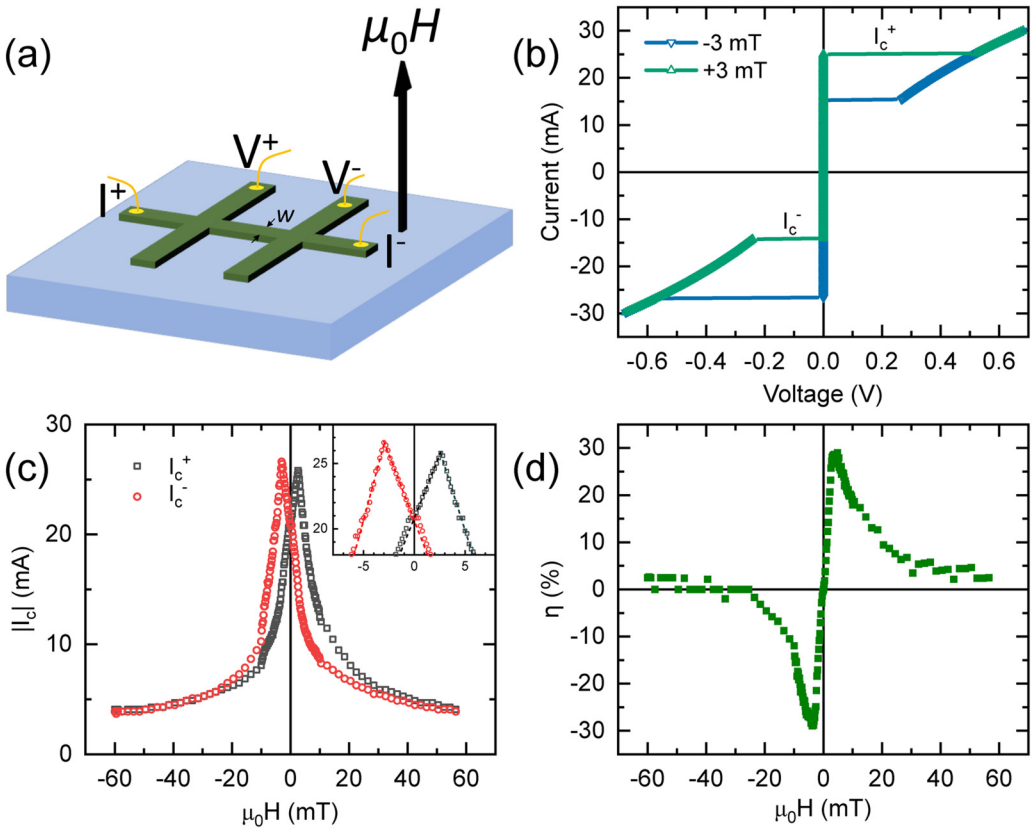

FIG. 1. Supercurrent diode effect in polycrystalline 65 nm thick Nb patterned into a 4 μm wide track, measured at 5 K. (a) Schematic cross section of the Nb track device showing the applied field and measurement current direction (not to scale). (b) Current–voltage characteristic of the device measured at the ± 3 mT applied out-of-plane field. (c) Extracted critical currents (I_c^+ and I_c^-) with the out-of-plane applied field, the inset shows the low field region with fitting to the model described in the text. The uncertainty in determining I_c is the current step size and is smaller than the data points. (d) Diode efficiency η corresponding to the dataset in (c).

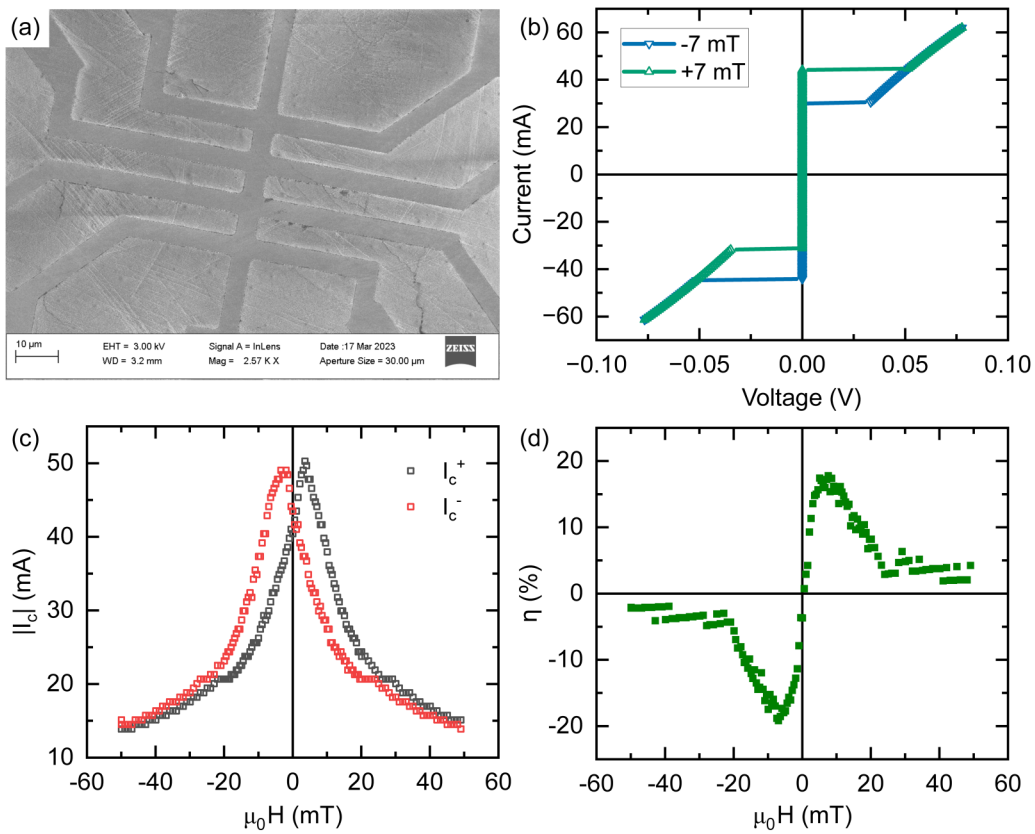

FIG. 2. Supercurrent diode effect in epitaxial 65 nm thick Nb. (a) Scanning electron microscope image of a 4 μm wide track. (b)–(d) Electrical transport characteristic of a 4 μm wide track, measured at 5 K. (a) Current–voltage characteristic of the device measured at ± 7 mT applied out-of-plane field. (b) Extracted critical currents (I_c^+ and I_c^-) with the out-of-plane applied field. The uncertainty in determining I_c is the current step size and is smaller than the data points. (c) Diode efficiency η corresponding to the dataset in (b).

polycrystalline Nb samples. Considering first the epitaxial sample, Fig. 3(a), two samples of at $w = 7$ and 10 μm did not show finite η. In these two tracks, I_c at low temperatures exceeded the maximum output of our current source (100 mA), limiting the range of temperatures we could measure. For the narrower samples which showed η, the temperature dependence shows similar trends for all samples, with the largest η at 1.8 K, and η decreasing with warming.

Figures 3(b) and 3(c) presents the track width dependence of η at fixed temperature. At 1.8 K, a clear peak in η is found for the 4 μm track, with η decreasing linearly for narrower or wider tracks. At 5 K, the peak in η is broader, with $w = 4$ and 5 μm showing similar η. Again, for narrower or wider tracks η decreases linearly with width. Linear fits the decay of η for tracks of 4, 5, 6, and 7 μm are presented as dashed lines.

In the polycrystalline Nb samples, Fig. 3(d), tracks in the width regime $3 \leq w \leq 5\,\mu$m follow a similar temperature trend where η is the largest for temperatures of 4 or 5 K and decreases from the maximum value as the temperature is cooled or warmed. Tracks with $w \geq 7\,\mu$m show the largest η at the lowest temperature, with η decreasing as the temperature is warmed. Considering the track width dependence of η at fixed temperature, Figs. 3(e) and 3(f), η shows the largest value for tracks of $w = 3$ or 4 μm. Upon increasing w, η decreases linearly between $7 \leq w \leq 10\,\mu$m at 1.8 K and between $5 \leq w \leq 10\,\mu$m at 1.8 K. The 5 μm track at 1.8 K is a outlier to this trend. Linear fits to the decay of η for tracks of 7, 8, and 10 μm are presented as dashed lines.

In an attempt to further understand the origin of the diode effect and the role of vorticies, we perform initialization experiments on one of our tracks. Figure 4 shows the epitaxial 65 nm thick Nb sample with 5 μm wide track at 6 K. (a)–(f) shows the initial state of the device after the zero applied field cools and the conditions necessary to initialize the supercurrent diode effect in the device. At the zero field cooled condition in Fig. 4(a), the device already shows a small diode effect of $\eta = 6\%$, presumably due to the small trapped flux in the superconducting magnet. Figures 4(a)–4(f) present the results of performing sequentially larger field sweeps. Starting from the zero applied field, we observe a crossover in I_c^+/I_c^- at approximately 1 mT. The crossover at 1 mT, where $\eta = 0$, likely corresponds to the true zero field condition.

Trapped magnetic flux is a common feature of superconducting coils. Here, we choose not to perform background subtraction of this effect, and we present the dataset "as measured." Due to the larger field step size used to acquire the data presented in Figs. 1 and 2, the small trapped flux is not visible in those datasets. A further consequence of the trapped flux is that our devices will have been cooled through the superconducting transition in a small magnetic field, which will contribute flux vorticies in the as cooled state. The dependence of the diode effect on field cooling was not investigated in this study. The maximum in I_c^+ is at about 4 mT. As in Figs. 1 and 2, the maximum diode effect, η, corresponds to the maximum in I_c^+. At larger fields, the effect reduces, and $I_c^+ = I_c^-$ at about 20 mT.

In Fig. 4, comparing the out and return field sweep directions, there is a hysteretic behavior in I_c and, hence, η. Considering Fig. 4(e), the hysteresis is particularly observable in I_c^+ between 10 and 20 mT but is present over the whole field range where $\eta \neq 0$. The hysteretic behavior with field history suggests that the diode effect is sensitive to the field history of the track. We expect that the preceding field history establishes different vortex states in the track, which, therefore, influences the magnitude of η. The largest hysteresis between 10 and 20 mT is reproduced in subsequent larger field sweeps [Fig. 4(f)].

IV. DISCUSSION

From the presented experimental data, we can report three key experimental observations. First, at 65 nm thick, our films are in a distinct mid-range thickness with respect to other works in the field.[43,48] In this mid-range thickness, we have shown that a diode effect is possible. Second, by varying the width of the tracks, we observe an unexpected dependence of the diode effect with track width. Third, we extend previous work,[48] which considered only epitaxial Nb and demonstrate that the supercurrent diode effect is present in both polycrystalline and epitaxial Nb.

In our polycrystalline Nb, the coherence length is 11.6 nm,[54] which is much less than the thickness of the 65 nm film studied here. Our results, therefore, suggest that the supercurrent diode effect reported here does not rely upon subtle interfacial effects, which may play an increasing role when the film thickness is comparable to the coherence length. An added benefit of using thicker films is that at 65 nm, Nb has a near bulk T_c, which makes our devices useful for integrating with Nb-based computing schemes operating at 4.2 K.

Our data show that the induced supercurrent diode effect depends upon the width of the track. From our data, we can estimate the upper limit of track width for the supercurrent diode effect. For the polycrystalline film, extrapolating the linear fit shown in Figs. 3(e) and 3(f) $\eta = 0$ for w between about 12 and 13 μm. In the epitaxial film, $\eta = 0$ is observed at 5 K for $w = 7\,\mu$m. Extrapolating the data at 1.8 K suggests that $\eta = 0$ for $w \approx 8\,\mu$m. In the epitaxial sample, η also reduces in the narrowest tracks, but this trend is not reproduced in the polycrystalline sample.

We propose that the induced diode effect does result from asymmetric properties in the two edges of our tracks. This

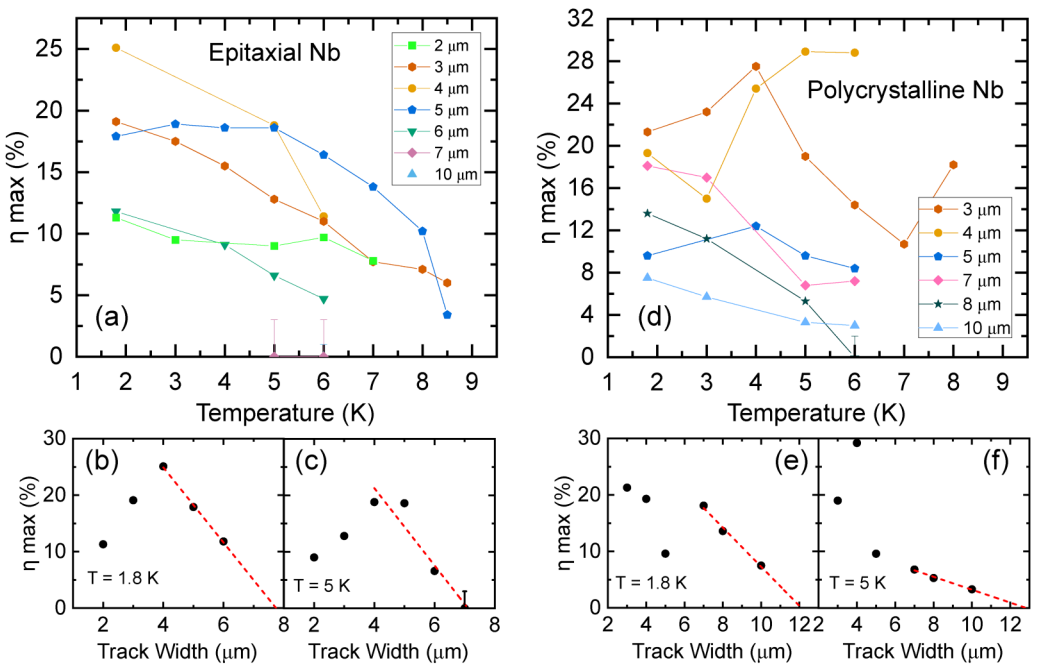

FIG. 3. Supercurrent diode effect in epitaxial and polycrystalline 65 nm thick Nb patterned into tracks (a) and (d) The maximum diode efficiency parameter, η, with temperature for a series of tracks with varying width for the epitaxial and polycrystalline samples, respectively. (b), (c) ,(e), and (f) Corresponding track width dependence of η at (b) and (e) 1.8 K and (c) and (f) 5 K. Solid lines in (a) and (d) represent guides for the eye, while dashed lines in (b), (c), (e), and (f) show linear fits the decay of η for the widest tracks.

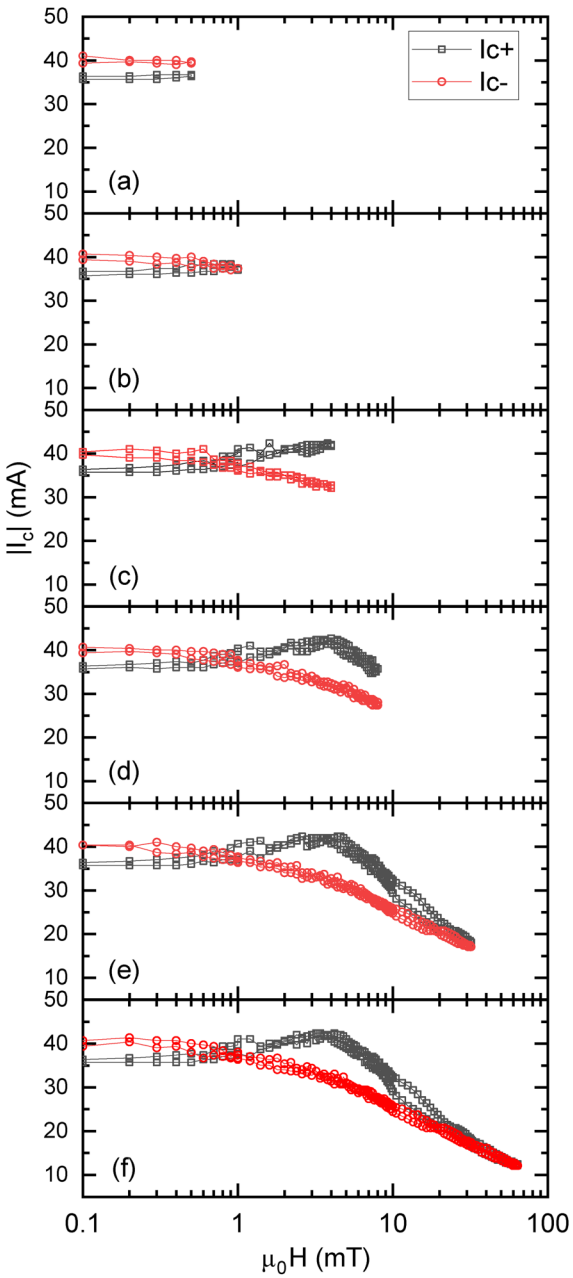

FIG. 4. Initialization of the supercurrent diode effect in epitaxial 65 nm thick Nb patterned into 5 μm wide track at 6 K. (a)–(e) I_c^+/I_c^- with sequentially larger field sweeps on a semi-log scale. Before each sweep, the sample was briefly warmed above T_c and cooled again in the zero applied field. The uncertainty in determining I_c is the current step size and is smaller than the data points.

asymmetry causes unequal generation, penetration, and expulsion of vortices on the two edges of the tracks, resulting in the observed rectification. Each edge has a different critical current density required for penetration of magnetic vortices, j_{pen}. This could be

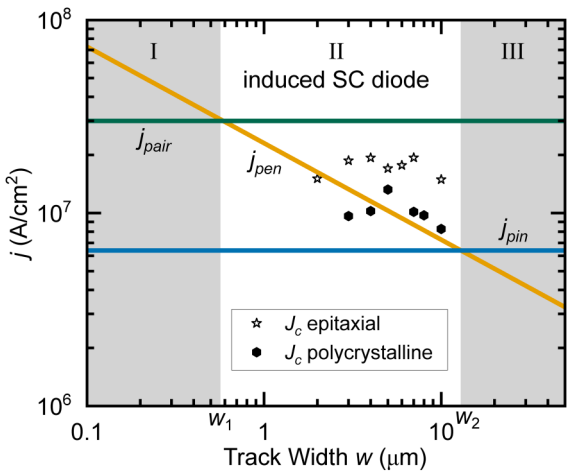

FIG. 5. Width dependence of the critical current densities in Nb tracks. Experimental data for the nominal critical current density at 5 K for all devices in this study. The polycrystalline tracks are fit to Eq. (1), with a best-fit value $B_{pen} = 11 \pm 1$ mT. Also shown are literature values for polycrystalline Nb depairing current[56] (j_{pair}) and depinning current[57] (j_{pin}). We define three regions depending on which mechanism determines the critical current density of our tracks, see text.

induced by the asymmetric edge roughness mechanism of Hou *et al.*[48] or, more generally, by any local changes in the superconducting gap such as, most probably, the edge profile. The diode effect in our tracks, therefore, relies on being in a regime where the critical current density (j_c) of the tracks is limited by flux vortice entry. We know this to be the case from our analysis of the $I_c(B)$ dependence of Fig. 1(c), inset. The requirement for the track to go normal is, therefore, flux penetrating the track from the edge barriers continuously and flux vortices moving freely across the track without being pinned.

There are three possible mechanisms to limit the critical current density j_c of our superconducting tracks. The ultimate limit is the depairing current, j_{pair}. Where the critical current of the track is limited by flux vortices, the critical current density is limited by the greater of the current density required for penetration of magnetic vortices, j_{pen}, and the current density required to depin the vortices, j_{pin}.

For our Nb tracks, we can reasonably assume that j_{pair} is an intrinsic material property and j_{pin} is a property of the film, both of which do not depend on track width. On the other hand, it has been shown that j_{pen} depends on the track width (w) according to[56]

$$j_{pen} = \frac{2\pi B_{pen}}{\mu_0 \sqrt{dw}}, \tag{1}$$

where d is the film thickness, B_{pen} is the minimum field for vortex penetration, and μ_0 is the magnetic permeability of free space. Figure 5 shows the experimentally determined maximum nominal j_c at 5 K for both the epitaxial and polycrystalline Nb tracks. j_{pen} is fitted to the polycrystalline dataset with B_{pen} a free fitting parameter,

returning a best-fit value of 11 ± 1 mT. Note that B_{pen} is likely a combination of the applied and self-magnetic fields in our system. Also plotted are the experimentally determined j_{pair} from Il'in *et al.* for narrow polycrystalline Nb tracks[56] and j_{pin} from Zhu *et al.* for a 110 nm polycrystalline Nb film.[57]

Considering the fit to the polycrystalline Nb tracks, it is possible to divide Fig. 5 into three width regions. For narrow tracks occupying region I ($w < w_1$), the critical current density in the track is limited by j_{pair}. Since vortices do not contribute to j_c, our conjecture is that it is not possible for fabrication to induce a supercurrent diode effect in this region. For intermediate region II ($w_1 < w < w_2$), the critical current is limited by j_{pen}. In this region, the track goes normal when the transport current equals j_{pen}, and a diode effect can be induced by device fabrication if j_{pen} is asymmetric on each edge. For wide tracks in region III ($w > w_2$), the critical current is no longer limited by j_{pen}. Here, upon applying a transport current, first vortices enter the track at the edges at transport current exceeding j_{pen}. However, these vortices become pinned, preventing the track from going normal. It is only when the transport current exceeds j_{pin} that vortices can move and the track goes normal. In region III, the induced diode effect should be suppressed as j_{pin} is an intrinsic material property and, therefore, likely to be uniform across the width of the track.

Comparing the width dependence of j_c in Fig. 5 to our experimental data on the width dependence of the supercurrent diode effect in Fig. 3, we can make the following observations and predictions. We expect that the induced diode effect will be suppressed in region III, which for the polycrystalline dataset is at $w \approx 13\,\mu$m. This width corresponds well with our extrapolation to $\eta = 0$ in Figs. 3(e) and 3(f). We can also use the model to predict that $w = 600$ nm is the upper boundary of region I for polycrystalline Nb. Therefore, tracks narrower than about 600 nm should not show an induced supercurrent diode effect, however, fabrication of tracks that narrow would require a change in fabrication methodology. Finally, applying similar analysis to the epitaxial Nb tracks, we conclude that both j_{pen} and j_{pin} must be higher in the epitaxial Nb. Interestingly, a higher j_{pen} would suggest that region I extends to wider epitaxial tracks compared to polycrystalline tracks, which would be consistent with our observation of reduced η in the narrowest epitaxial tracks in Figs. 3(b) and 3(c).

V. CONCLUSIONS

In conclusion, we report on the induced supercurrent diode effect in 65 nm thick polycrystalline and epitaxial Nb films patterned into tracks. Consistent with previous works, the superconductor itself does not require any intrinsic inversion symmetry breaking and the layer can be significantly thicker than the coherence length. Our experimental results and model suggest that in order to distinguish between the intrinsic and induced supercurrent diode effect in a materials system, the critical current density in the fabricated devices should be limited by j_{pair} and not by flux vortices. Therefore, claims of the intrinsic diode effect should only be made for devices limited by j_{pair} (occupying region I of Fig. 5). This is particularly relevant for the study of exotic materials to isolate the proposed intrinsic effect from the fabrication induced effect we report here.

For technological applications, it would be possible to manipulate the devices edges to create local differences in j_{pen}, for example, by engineering edge roughness or by changing the superconducting properties of one edge by ion implantation and, therefore, control induced diode effects.

Our largest reported diode efficiency is $\eta \approx 30\%$ in a 4 μm wide track at 5 K. We report that the supercurrent diode effect can be observed in Nb tracks over a range of track widths applied out-of-plane applied fields and temperatures. Our results show a track width dependence, where for the widest tracks in this study, we report that the diode effect reduces or disappears altogether. We present a model of the critical currents in the track to account for our observed width dependence.

ACKNOWLEDGMENTS

The work was supported financially through the following EPSRC Grant (No. EP/V028138/1). We acknowledge support from the Henry Royce Institute. We would like to thank N.O. Birge for helpful discussions.

AUTHOR DECLARATIONS

Conflict of Interest

The authors have no conflicts to disclose.

Author Contributions

N Satchell: Conceptualization (lead); Formal analysis (lead); Funding acquisition (supporting); Investigation (lead); Methodology (lead); Writing – original draft (lead); Writing – review & editing (equal). **PM Shepley:** Investigation (supporting); Methodology (supporting); Writing – review & editing (equal). **MC Rosamond:** Investigation (supporting); Methodology (supporting); Writing – review & editing (equal). **G Burnell:** Conceptualization (equal); Funding acquisition (lead); Investigation (supporting); Methodology (supporting); Project administration (lead); Writing – review & editing (equal).

DATA AVAILABILITY

The datasets generated during the current study are available in the University of Leeds repository at https://doi.org/10.5518/1293, Ref. 58.

REFERENCES

[1]P. S. Swartz and H. R. Hart, "Asymmetries of the critical surface current in type-II superconductors," Phys. Rev. **156**, 412–420 (1967).
[2]N. Touitou, P. Bernstein, J. F. Hamet, C. Simon, L. Méchin, J. P. Contour, and E. Jacquet, "Nonsymmetric current–voltage characteristics in ferromagnet/superconductor thin film structures," Appl. Phys. Lett. **85**, 1742–1744 (2004).
[3]D. Y. Vodolazov, B. A. Gribkov, S. A. Gusev, A. Y. Klimov, Y. N. Nozdrin, V. V. Rogov, and S. N. Vdovichev, "Considerable enhancement of the critical current in a superconducting film by a magnetized magnetic strip," Phys. Rev. B **72**, 064509 (2005).
[4]M. Morelle and V. V. Moshchalkov, "Enhanced critical currents through field compensation with magnetic strips," Appl. Phys. Lett. **88**, 172507 (2006).
[5]A. Papon, K. Senapati, and Z. H. Barber, "Asymmetric critical current of niobium microbridges with ferromagnetic stripe," Appl. Phys. Lett. **93**, 172507 (2008).

[6]R. Grein, M. Eschrig, G. Metalidis, and G. Schön, "Spin-dependent cooper pair phase and pure spin supercurrents in strongly polarized ferromagnets," Phys. Rev. Lett. **102**, 227005 (2009).
[7]K. Halterman, M. Alidoust, R. Smith, and S. Starr, "Supercurrent diode effect, spin torques, and robust zero-energy peak in planar half-metallic trilayers," Phys. Rev. B **105**, 104508 (2022).
[8]Y. Zhang, Y. Gu, P. Li, J. Hu, and K. Jiang, "General theory of Josephson diodes," Phys. Rev. X **12**, 041013 (2022).
[9]M. Davydova, S. Prembabu, and L. Fu, "Universal Josephson diode effect," Sci. Adv. **8**, eabo0309 (2022).
[10]M. Eschrig, "Spin-polarized supercurrents for spintronics: A review of current progress," Rep. Prog. Phys. **78**, 104501 (2015).
[11]V. Braude and Y. V. Nazarov, "Fully developed triplet proximity effect," Phys. Rev. Lett. **98**, 077003 (2007).
[12]D. M. Heim, N. G. Pugach, M. Y. Kupriyanov, E. Goldobin, D. Koelle, and R. Kleiner, "Ferromagnetic planar Josephson junction with transparent interfaces: A ϕ junction proposal," J. Phys.: Condens. Matter **25**, 215701 (2013).
[13]E. Goldobin, D. Koelle, and R. Kleiner, "Tunable $\pm\varphi$, φ_0, and $\varphi_0 \pm \varphi$ Josephson junction," Phys. Rev. B **91**, 214511 (2015).
[14]Y. M. Shukrinov, I. R. Rahmonov, and K. Sengupta, "Ferromagnetic resonance and magnetic precessions in φ_0 junctions," Phys. Rev. B **99**, 224513 (2019).
[15]A. Mazanik, I. Rahmonov, A. Botha, and Y. Shukrinov, "Analytical criteria for magnetization reversal in a φ_0 Josephson junction," Phys. Rev. Appl. **14**, 014003 (2020).
[16]H. Meng, X. Wu, Y. Ren, and J. Wu, "Anomalous supercurrent modulated by interfacial magnetizations in Josephson junctions with ferromagnetic bilayers," Phys. Rev. B **106**, 174502 (2022).
[17]I. V. Bobkova, A. M. Bobkov, A. A. Zyuzin, and M. Alidoust, "Magnetoelectrics in disordered topological insulator Josephson junctions," Phys. Rev. B **94**, 134506 (2016).
[18]M. Alidoust and H. Hamzehpour, "Spontaneous supercurrent and φ_0 phase shift parallel to magnetized topological insulator interfaces," Phys. Rev. B **96**, 165422 (2017).
[19]M. Y. Li, Y. Yang, J. G. Hu, T. M. Liu, and Y. C. Tao, "Anomalous Josephson current through a topological noncoplanar ferromagnetic trilayer," J. Phys.: Condens. Matter **34**, 135801 (2022).
[20]M. Alidoust, "Self-biased current, magnetic interference response, and superconducting vortices in tilted Weyl semimetals with disorder," Phys. Rev. B **98**, 245418 (2018).
[21]M. Alidoust and K. Halterman, "Evolution of pair correlation symmetries and supercurrent reversal in tilted Weyl semimetals," Phys. Rev. B **101**, 035120 (2020).
[22]K. Kulikov, D. Sinha, Y. M. Shukrinov, and K. Sengupta, "Josephson junctions of Weyl and multi-Weyl semimetals," Phys. Rev. B **101**, 075110 (2020).
[23]D. Sinha, "Josephson effect in type-I Weyl semimetals," Phys. Rev. B **102**, 085144 (2020).
[24]M. Alidoust, "Critical supercurrent and φ_0 state for probing a persistent spin helix," Phys. Rev. B **101**, 155123 (2020).
[25]M. Alidoust, C. Shen, and I. Žutić, "Cubic spin-orbit coupling and anomalous Josephson effect in planar junctions," Phys. Rev. B **103**, L060503 (2021).
[26]D. Monroe, M. Alidoust, and I. Žutić, "Tunable planar Josephson junctions driven by time-dependent spin-orbit coupling," Phys. Rev. Appl. **18**, L031001 (2022).
[27]M. H. S. Amin, A. N. Omelyanchouk, and A. M. Zagoskin, "Mechanisms of spontaneous current generation in an inhomogeneous *d*-wave superconductor," Phys. Rev. B **63**, 212502 (2001).
[28]T. Liu, L. Zhou, and Y. C. Tao, "Anomalous Josephson effect modulated by magnetic misorientation in a topological unconventional superconductor hybrid structure," EPL **136**, 17004 (2021).
[29]Y.-M. Xie, D. K. Efetov, and K. T. Law, "Valley-polarized state induced φ_0-Josephson junction in twisted bilayer graphene" arXiv:2202.05663[cond-mat.mes-hall] (2022).
[30]B. Pal, A. Chakraborty, P. K. Sivakumar, M. Davydova, A. K. Gopi, A. K. Pandeya, J. A. Krieger, Y. Zhang, S. Ju, N. Yuan, N. B. M. Schröter, L. Fu, and S. S. P. Parkin, "Josephson diode effect from Cooper pair momentum in a topological semimetal," Nat. Phys. **18**, 1228–1233 (2022).
[31]C. Baumgartner, L. Fuchs, A. Costa, S. Reinhardt, S. Gronin, G. C. Gardner, T. Lindemann, M. J. Manfra, P. E. Faria Junior, D. Kochan, and J. Fabian, "Supercurrent rectification and magnetochiral effects in symmetric Josephson junctions," Nat. Nanotechnol. **17**, 39–44 (2022).
[32]H. Wu, Y. Wang, Y. Xu, P. K. Sivakumar, C. Pasco, U. Filippozzi, S. S. Parkin, Y.-J. Zeng, T. McQueen, and M. N. Ali, "The field-free Josephson diode in a van der Waals heterostructure," Nature **604**, 653–656 (2022).
[33]T. Golod and V. M. Krasnov, "Demonstration of a superconducting diode-with-memory, operational at zero magnetic field with switchable nonreciprocity," Nat. Commun. **13**, 3658 (2022).
[34]K.-R. Jeon, J.-K. Kim, J. Yoon, J.-C. Jeon, H. Han, A. Cottet, T. Kontos, and S. S. Parkin, "Zero-field polarity-reversible Josephson supercurrent diodes enabled by a proximity-magnetized Pt barrier," Nat. Mater. **21**, 1008–1013 (2022).
[35]B. Turini, S. Salimian, M. Carrega, A. Iorio, E. Strambini, F. Giazotto, V. Zannier, L. Sorba, and S. Heun, "Josephson diode effect in high-mobility InSb nanoflags," Nano Lett. **22**, 8502–8508 (2022).
[36]A. Daido, Y. Ikeda, and Y. Yanase, "Intrinsic superconducting diode effect," Phys. Rev. Lett. **128**, 037001 (2022).
[37]N. F. Yuan and L. Fu, "Supercurrent diode effect and finite-momentum superconductors," Proc. Natl. Acad. Sci. **119**, e2119548119 (2022).
[38]T. Karabassov, I. V. Bobkova, A. A. Golubov, and A. S. Vasenko, "Hybrid helical state and superconducting diode effect in superconductor/ferromagnet/topological insulator heterostructures," Phys. Rev. B **106**, 224509 (2022).
[39]B. Zhai, B. Li, Y. Wen, F. Wu, and J. He, "Prediction of ferroelectric superconductors with reversible superconducting diode effect," Phys. Rev. B **106**, L140505 (2022).
[40]A. Daido and Y. Yanase, "Superconducting diode effect and nonreciprocal transition lines," Phys. Rev. B **106**, 205206 (2022).
[41]H. D. Scammell, J. I. A. Li, and M. S. Scheurer, "Theory of zero-field superconducting diode effect in twisted trilayer graphene," 2D Mater. **9**, 025027 (2022).
[42]D. Wang, Q.-H. Wang, and C. Wu, "Symmetry constraints on direct-current josephson diodes," arXiv:2209.12646[cond-mat.supr-con] (2022).
[43]F. Ando, Y. Miyasaka, T. Li, J. Ishizuka, T. Arakawa, Y. Shiota, T. Moriyama, Y. Yanase, and T. Ono, "Observation of superconducting diode effect," Nature **584**, 373–376 (2020).
[44]R. Wakatsuki, Y. Saito, S. Hoshino, Y. M. Itahashi, T. Ideue, M. Ezawa, Y. Iwasa, and N. Nagaosa, "Nonreciprocal charge transport in noncentrosymmetric superconductors," Sci. Adv. **3**, e1602390 (2017).
[45]E. Zhang, X. Xu, Y.-C. Zou, L. Ai, X. Dong, C. Huang, P. Leng, S. Liu, Y. Zhang, Z. Jia, and X. Peng, "Nonreciprocal superconducting $NbSe_2$ antenna," Nat. Commun. **11**, 1–9 (2020).
[46]H. Narita, J. Ishizuka, R. Kawarazaki, D. Kan, Y. Shiota, T. Moriyama, Y. Shimakawa, A. V. Ognev, A. S. Samardak, Y. Yanase, and T. Ono, "Field-free superconducting diode effect in noncentrosymmetric superconductor/ferromagnet multilayers," Nat. Nanotechnol. **17**, 823–828 (2022).
[47]J.-X. Lin, P. Siriviboon, H. D. Scammell, S. Liu, D. Rhodes, K. Watanabe, T. Taniguchi, J. Hone, M. S. Scheurer, and J. Li, "Zero-field superconducting diode effect in small-twist-angle trilayer graphene," Nat. Phys. **18**, 1221–1227 (2022).
[48]Y. Hou, F. Nichele, H. Chi, A. Lodesani, Y. Wu, M. F. Ritter, D. Z. Haxell, M. Davydova, S. Ilić, F. S. Bergeret, and A. Kamra, "Ubiquitous superconducting diode effect in superconductor thin films," arXiv:2205.09276 (2022).
[49]D. Suri, A. Kamra, T. N. G. Meier, M. Kronseder, W. Belzig, C. H. Back, and C. Strunk, "Non-reciprocity of vortex-limited critical current in conventional superconducting micro-bridges," Appl. Phys. Lett. **121**, 102601 (2022).
[50]S. Ustavschikov, M. Y. Levichev, I. Y. Pashenkin, N. Gusev, S. Gusev, and D. Y. Vodolazov, "Diode effect in a superconducting hybrid Cu/MoN strip with a lateral cut," J. Exp. Theor. Phys. **135**, 226–230 (2022).
[51]A. Gutfreund, H. Matsuki, V. Plastovets, A. Noah, L. Gorzawski, N. Fridman, G. Yang, A. Buzdin, O. Millo, J. W. Robinson, and Y. Anahory, "Direct observation of a superconducting vortex diode," Nat. Commun. **14**, 1630 (2023).

[52]D. Y. Vodolazov and F. M. Peeters, "Superconducting rectifier based on the asymmetric surface barrier effect," Phys. Rev. B **72**, 172508 (2005).
[53]The Royce Deposition System is a multi-chamber, multi-technique thin film deposition tool based at the University of Leeds as part of the Henry Royce Institute.
[54]P. Quarterman, N. Satchell, B. J. Kirby, R. Loloee, G. Burnell, N. O. Birge, and J. A. Borchers, "Distortions to the penetration depth and coherence length of superconductor/normal-metal superlattices," Phys. Rev. Mater. **4**, 074801 (2020).
[55]A. Suter, E. Morenzoni, N. Garifianov, R. Khasanov, E. Kirk, H. Luetkens, T. Prokscha, and M. Horisberger, "Observation of nonexponential magnetic penetration profiles in the Meissner state: A manifestation of nonlocal effects in superconductors," Phys. Rev. B **72**, 024506 (2005).
[56]K. Il'in, D. Rall, M. Siegel, A. Engel, A. Schilling, A. Semenov, and H.-W. Huebers, "Influence of thickness, width and temperature on critical current density of Nb thin film structures," Phys. C: Supercond. Appl. **470**, 953–956 (2010).
[57]J. Zhu, J. Lockhart, and J. Turneare, "Pinning forces in a disk-shaped superconducting niobium film," Phys. B: Condens. Matter **194–196**, 1357–1358 (1994).
[58]N. Satchell, P. M. Shepley, M. C. Rosamond, and G. Burnell (2023). "Supercurrent diode effect in thin film Nb tracks," Dataset. https://doi.org/10.5518/1293